SURFACE METHODS FOR THE COMPUTATION OF CHARGED-PARTICLE TRANSFER MAPS FROM MAGNETIC FIELD DATA

C. E. Mitchell*, Lawrence Berkeley National Laboratory, Berkeley, CA 94729, USA
A. J. Dragt, University of Maryland, College Park, MD 94720, USA

Abstract

The behavior of orbits in charged-particle beam transport systems, including both linear and circular accelerators as well as final focus sections and spectrometers, can depend sensitively on nonlinear fringe-field and high-order-multipole effects in the various beam-line elements. Surface fitting algorithms provide a robust and reliable method for extracting this information accurately from 3-dimensional field data provided on a grid. Based on these realistic field models, Lie or other methods may be used to compute accurate design orbits and high-order symplectic maps about these orbits. We describe the implementation of a general method for treating magnetic elements with curved reference trajectories that is especially well-suited for extracting symplectic transfer maps for large-sagitta bending dipoles with fringe fields.

INTRODUCTION

Successful design of high-performance free-electron lasers, storage rings, and colliders relies heavily on charged-particle optics codes with high-order nonlinear tracking and map capabilities. To compute design orbits and high-order transfer maps (in Lie or Taylor form) that accurately include the effects of asymmetries, nonlinear fringe-fields and high-order multipoles not well-captured by idealized magnet and cavity models, realistic 3-dimensional electric and magnetic field information for various beam-line elements is needed. Realistic field data can be provided on a grid by 3D finite element codes, sometimes spot checked against measured data. However, the computation of high-order transfer maps requires high derivatives of the fields or corresponding potentials, and the direct calculation of high derivatives based only on grid data is intolerably sensitive to noise (due to truncation or round-off) in the grid data.

The effect of numerical noise can best be overcome by fitting onto a bounding surface far from the beam axis and continuing inward using the Maxwell equations [1–4]. While the process of differentiation amplifies the effect of numerical noise, the process of continuing inward using the Maxwell equations is *smoothing*. For beam-line elements such as quadrupoles, sextupoles, octupoles, wigglers, and RF cavities, well-established algorithms exist that employ cylindrical fitting surfaces with circular, elliptical, or rectangular cross section [1, 3–5] to extract transfer maps to high order. These algorithms are robust and insensitive to noise in the underlying grid data, but are limited to beamline elements with straight or nearly-straight reference trajectories.

In this paper we describe a parallel code (BMAP3D) designed to extract symplectic transfer maps in Lie-algebraic form from 3D field data associated with curved magnetic elements, such as dipoles with large design-orbit sagitta. The data is fitted onto a bent box with straight ends that extends into the fringe-field regions outside the beam-line element, and the resulting map takes into account all fringe-field effects as well as all linear and nonlinear effects up to the desired order. We work with the canonical equations of motion based on a computed vector potential $\mathbf{A}$. If instead one wishes to integrate noncanonical equations employing the magnetic field $\boldsymbol{B}$, it can be obtained using $\boldsymbol{B} = \nabla \times \boldsymbol{A}$. The technique described is quite general, and can be applied to magnetic elements with complex reference trajectories (which need not be known exactly) and more complex surface-fitting geometries.

SURFACE REPRESENTATION OF FIELDS AND POTENTIALS

Consider a volume V free of electromagnetic sources and contained within the beam-line element of interest, and let S denote its boundary surface. The solution of Maxwell's equations for a single mode with time dependence $\exp(-i\omega t)$ can be represented in terms of field values on the surface S. Defining a function Φ by

$$\Phi(\mathbf{r}, \mathbf{r}') = \frac{e^{ik|\mathbf{r}-\mathbf{r}'|}}{4\pi|\mathbf{r}-\mathbf{r}'|}, \qquad k = \omega/c, \tag{1}$$

we have for points $\mathbf{r}$ interior to V that [6]:

$$\begin{aligned}\mathbf{E}(\mathbf{r}) &= -\int_S \{i\omega(\mathbf{n}\times\mathbf{B})\Phi + (\mathbf{n}\times\mathbf{E})\times\nabla'\Phi + (\mathbf{n}\cdot\mathbf{E})\nabla'\Phi\}\, dS',\\ \mathbf{B}(\mathbf{r}) &= \int_S \left\{i\frac{\omega}{c^2}(\mathbf{n}\times\mathbf{E})\Phi - (\mathbf{n}\times\mathbf{B})\times\nabla'\Phi - (\mathbf{n}\cdot\mathbf{B})\nabla'\Phi\right\} dS',\end{aligned} \tag{2}$$

where $\mathbf{n}$ is the outward-directed normal at each point $\mathbf{r}'$ on the surface S. The representation (2) is smooth (analytic), and convergent Taylor series for $\mathbf{E}$ and $\mathbf{B}$ about any point interior to V may be obtained by expanding the integral kernel Φ in the unprimed variables $\mathbf{r}$. In this way, each coefficient in the Taylor series is represented as an integral over the boundary surface S.

Magnetic Vector Potential

In this paper, we consider only magnetic elements (with $\omega \to 0$, $\mathbf{E} \to 0$), and employ canonical equations of motion

* ChadMitchell@lbl.gov

Copyright © 2015 CC-BY-3.0 and by the respective authors

ISBN 978-3-95450-136-6

for which we require a vector potential $\mathbf{A}$ such that $\mathbf{B} = \nabla\times\mathbf{A}$. Using (2) and results related to Dirac monopoles, it can be shown [7, 8] that one can represent the vector potential in the volume V in the form $\mathbf{A} = \mathbf{A}^n + \mathbf{A}^t$, where:

$$\mathbf{A}^n(\mathbf{r}) = \int_S [\mathbf{n}\cdot\mathbf{B}(\mathbf{r}')]\mathbf{G}^n(\mathbf{r};\mathbf{r}',\mathbf{m})dS',$$
$$\mathbf{A}^t(\mathbf{r}) = \int_S \psi(\mathbf{r}')\mathbf{G}^t(\mathbf{r};\mathbf{r}',\mathbf{n})dS'. \quad (3)$$

Here ψ denotes a magnetic scalar potential with the property $\mathbf{B} = \nabla\psi$, which we assume to be known on the boundary surface. (If ψ is not known, it can be recovered from the components of $\mathbf{B}$ tangent to the surface.)

Here $\mathbf{n}$ denotes the unit normal at each surface point $\mathbf{r}'$, and $\mathbf{m}$ is an outward-directed unit vector at $\mathbf{r}'$ with the property that the ray $\{\mathbf{r}' + \lambda\mathbf{m} : \lambda > 0\}$ does not intersect the volume V. The vector-valued integration kernels $\mathbf{G}^n$ and $\mathbf{G}^t$ are given by [5, 8]

$$\mathbf{G}^n(\mathbf{r};\mathbf{r}',\mathbf{m}(\mathbf{r}')) = \frac{\mathbf{m}\times(\mathbf{r}-\mathbf{r}')}{4\pi|\mathbf{r}-\mathbf{r}'|(|\mathbf{r}-\mathbf{r}'| - \mathbf{m}\cdot(\mathbf{r}-\mathbf{r}'))},$$
$$\mathbf{G}^t(\mathbf{r};\mathbf{r}',\mathbf{n}(\mathbf{r}')) = \frac{\mathbf{n}\times(\mathbf{r}-\mathbf{r}')}{4\pi|\mathbf{r}-\mathbf{r}'|^3}. \quad (4)$$

It can be verified that each kernel $\mathbf{G}^\alpha$ has the two properties $\nabla\cdot\mathbf{G}^\alpha = 0$ and $\nabla\times\nabla\times\mathbf{G}^\alpha = 0$ within the region of interest, where derivatives are taken with respect to the variable $\mathbf{r}$. As a result, the vector potential $\mathbf{A}$ given by (3) shares these properties. It follows that $\nabla\cdot\mathbf{B} = 0$ and $\nabla\times\mathbf{B} = 0$, and $\mathbf{A}$ satisfies the Coulomb gauge condition, for any surface values $\mathbf{n}\cdot\mathbf{B}$ and ψ, even if these values are noisy and the surface integrals are only evaluated approximately. Furthermore, $\mathbf{G}^n$ and $\mathbf{G}^t$ are analytic within the region of interest, and convergent Taylor series for $\mathbf{A}$ about any point interior to V may be obtained by expanding the integral kernels $\mathbf{G}^\alpha$ in the unprimed variables $\mathbf{r}$.

EXTRACTING MAPS USING BMAP3D

Consider a bending magnet with large design-orbit sagitta, and suppose that the values B_x, B_y, and B_z and ψ are provided on a 3D grid that lies within the magnet and extends into the magnet fringe field regions. We surround the design trajectory by a bent box with straight ends that encloses no iron or other sources (Fig. 1). If the data $\mathbf{B}$ and ψ are interpolated onto the boundary of the box, the result (3) allows one to construct a corresponding vector potential and its Taylor coefficients about any point in the interior via surface integrals, without the need for numerical differentiation. Knowledge of these quantities allows one to construct the Hamiltonian and its Taylor series near the design trajectory, which are sufficient to compute a symplectic transfer map through the magnet [9].

The code BMAP3D uses this technique to compute the design orbit and an associated transfer map about this orbit in Lie-algebraic form through third order for a given set of data B_x, B_y, B_z and ψ on a regular Cartesian grid. The

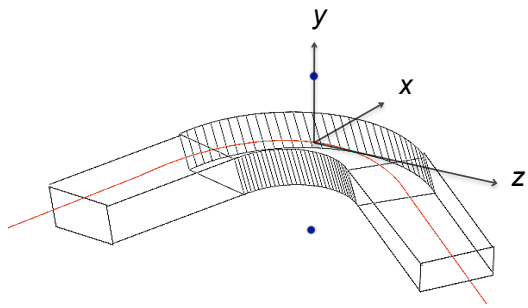

Figure 1: A bent box surrounding a reference trajectory (red) through the magnetic field of a bending dipole. The dots above and below the midplane illustrate the monopole doublet used to generate the magnetic field described in (6).

equations of motion for the design trajectory are integrated simultaneously with the equations for the Lie generators of the nonlinear map [9] using the global Cartesian coordinate system shown in Fig. 1, with z chosen as the independent variable. At each numerical step in z, the code uses efficient truncated power series algebra (TPSA) algorithms to compute the Taylor coefficients of the integral kernels (4) about the design point, which are used to extract the Taylor coefficients of $\mathbf{A}$ (through degree 4) by surface integrals of the form (3). In addition to the final transfer map, Taylor coefficients of $\mathbf{A}$ and $\mathbf{B}$ along the design trajectory are provided as numerical output.

Each Taylor coefficient of the vector potential $\mathbf{A}$ at a fixed value of z requires a single integration of the field and potential data over the surface S. Due to the computational cost associated with the number of Taylor coefficients required, the code has been parallelized using a domain decomposition by partitioning the surface of the bent box into disjoint regions. During the surface integration required for a given Taylor coefficient, integration over each region is performed on a separate processor core. This parallelization allows a large number of maps (~100) to be computed from distinct 3D data sets within a reasonable time (~hours), allowing for statistical studies or optimization of magnet design.

Benchmarks

The code is benchmarked using an exactly-soluble Maxwellian field that captures many features of a physical dipole. Suppose two magnetic monopoles having strengths $\pm g$ are placed at the (x, y, z) locations

$$r^+ = (0, a, 0),\ r^- = (0, -a, 0). \quad (5)$$

These monopoles generate a source-free magnetic field ($\nabla\times\mathbf{B} = 0$ and $\nabla\cdot\mathbf{B} = 0$) away from the two points (5). The field is given by $\mathbf{B} = \nabla\psi$ with:

$$\psi(x,y,z) = \psi_+(x,y,z) + \psi_-(x,y,z) =$$
$$-g[x^2 + (y-a)^2 + z^2]^{-1/2} + g[x^2 + (y+a)^2 + z^2]^{-1/2}. \quad (6)$$

In our test, $a = 2.5$ cm and $g = 1$ Tesla-(cm)^2. We set up a regular grid in x, y, z space, where $x \in [-4.4, 4.4]$

ISBN 978-3-95450-136-6

Copyright © 2015 CC-BY-3.0 and by the respective authors

with spacing $h_x = 0.1$, $y \in [-2.4, 2.4]$ with $h_y = 0.1$, and $z \in [-300, 300]$ with $h_z = 0.125$ (in units of cm). The values of B_x, B_y, B_z, and ψ are computed and stored at each grid point.

We choose an 8.65 MeV electron reference trajectory that lies in the midplane, which makes a 30 degree bend and passes directly through the midpoint joining the two monopoles (Fig. 1). We surround this reference trajectory by a bent box with height 4 cm and width 8 cm and a bending angle of 30 degrees. (The length of the arc segment is 10 cm, and the length of each straight leg is 3.054 m.) Using the code BMAP3D, power series for the components of **A** and **B** about each reference point $\mathbf{r}_d$ are computed from grid data and compared to the analytically known Taylor coefficients of the field.

The computed vector potential is shown in Fig. 2, and Fig. 3 illustrates the error in two third-order Taylor coefficients of the corresponding magnetic field. In each case, this error is measured relative to the maximum value attained by the coefficient along the reference trajectory. The increase in error near the endpoints $z = \pm 20$ cm is due to the fact that the contribution of the magnetic field and magnetic scalar potential on the two end faces of the bent box have been omitted, and this error can be reduced by allowing the straight legs of the box to extend farther into the fringe field region.

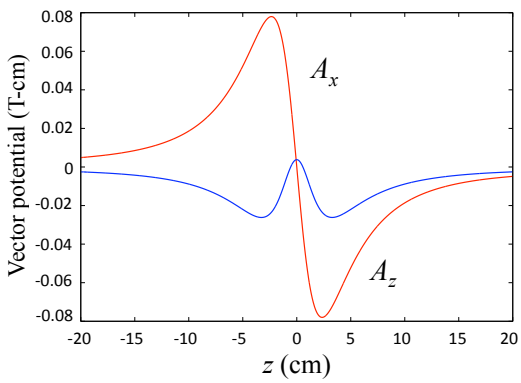

Figure 2: The vector potential for the monopole doublet for the case $a = 2.5$ cm and $g = 1$ Tesla-(cm)^2 at points along the reference trajectory, shown as a function of the longitudinal coordinate z. (Red) The component A_x. (Blue) The component A_z. Note that $A_y = 0$.

To benchmark the transfer map, a vector potential for the monopole doublet can be explicitly constructed in one simple gauge [5, 9]. Using this exactly-known vector potential, a reference trajectory can be computed and the transfer map determined using numerical integration of the map equations. This map can then be compared to the map obtained using the surface method just described. In this case, we find that the relative difference in each coefficient of the third-order transfer map is 10^{-4} or smaller.

Smoothing

The key feature of this technique is that results are relatively insensitive to numerical errors (noise) in the underlying grid data. To examine the effect of numerical noise, we generate random magnetic field errors $\Delta\mathbf{B}$ and potential errors $\Delta\psi$ at each grid point that are proportional, at the 1% level, to the magnetic field **B** and scalar potential ψ of the monopole doublet (6). At each mesh point (x_j, y_j, z_j) we set:

$$\Delta B_{x,y,z}(x_j, y_j, z_j) = \epsilon B_{x,y,z}(x_j, y_j, z_j)\delta_{x,y,z}(j), \quad (7a)$$

$$\Delta\psi(x_j, y_j, z_j) = \epsilon\psi(x_j, y_j, z_j)\delta_\psi(j). \quad (7b)$$

Here $\delta_x(j)$, $\delta_y(j)$, $\delta_z(j)$, and $\delta_\psi(j)$ are uniformly distributed random variables taking values in the interval $[-1, 1]$, and $\epsilon = 0.01$. Using the code BMAP3D, the values (7) are interpolated onto the surface of the bent box described in the previous Section, and the vector potential and its Taylor coefficients are computed about the reference trajectory shown in Fig. 1. The resulting vector potential components A_x and A_z are shown in Fig. 4 for six distinct random seeds (red). This procedure was performed for a total of 160 random seeds, and the rms values of A_x and A_z at each value of z are shown in blue, indicating maximum rms values that are 6×10^{-5} and 3×10^{-4} relative to the maximum values of A_x and A_z shown in Fig. 2. Thus, in the case of the monopole doublet, random noise of order 1% in the grid values produces a relative error in the computed vector potential that is only of order 10^{-4} along the reference

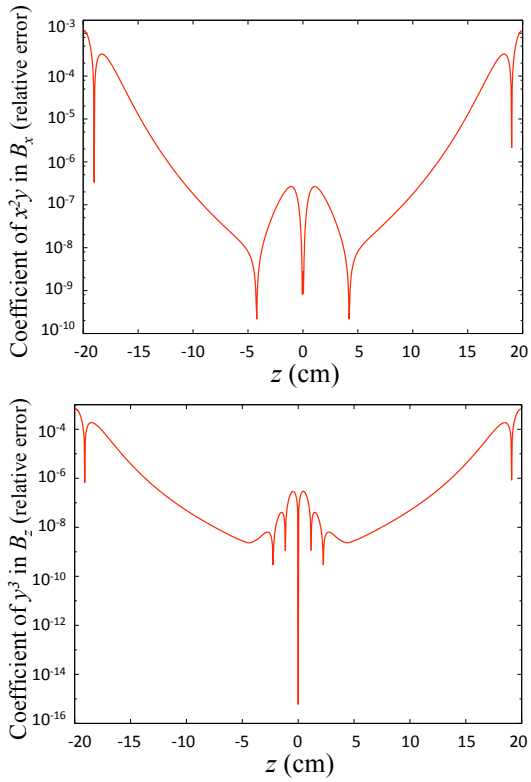

Figure 3: The error in the Taylor coefficients of the computed magnetic field of the monopole doublet (6) for the case $a = 2.5$ cm and $g = 1$ Tesla-(cm)^2 is shown along the reference trajectory as a function of the longitudinal coordinate z.

Copyright © 2015 CC-BY-3.0 and by the respective authors

ISBN 978-3-95450-136-6

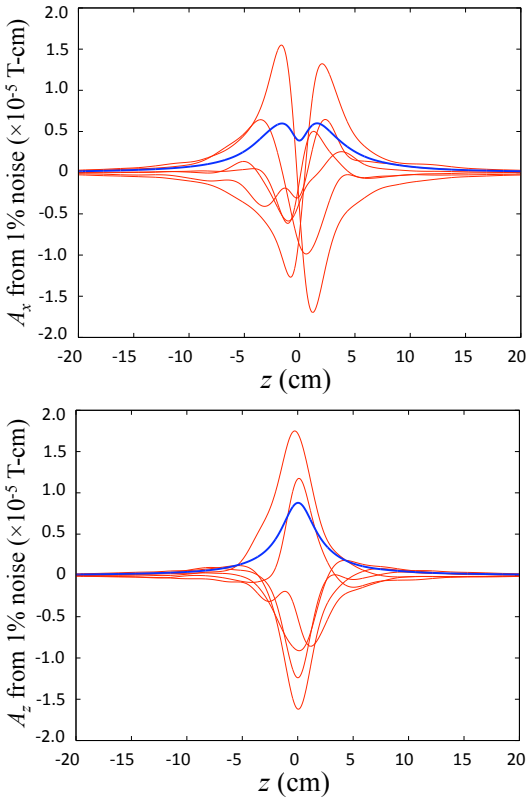

Figure 4: Vector potential components A_x and A_z computed from 1% random noise for the case $a = 2.5$ cm and $g = 1$ Tesla-(cm)^2. (Red) Results are shown for 6 distinct random seeds. (Blue) The rms value as computed using 160 random seeds.

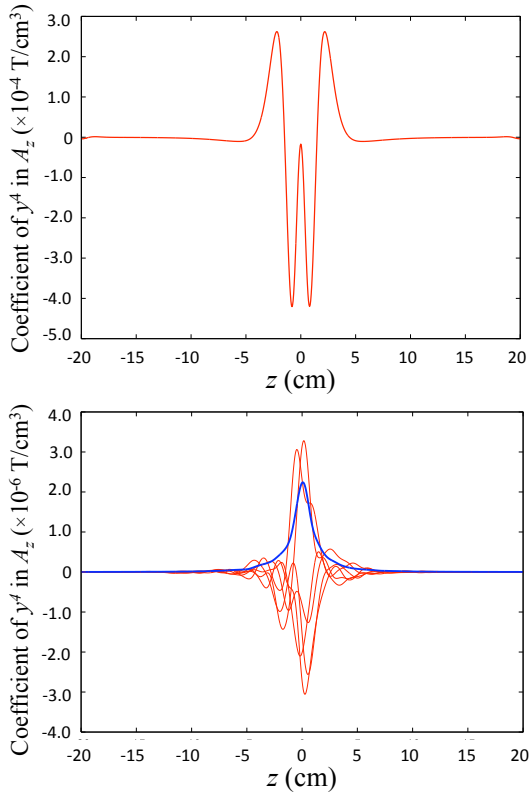

Figure 5: (Upper) The coefficient of the monomial y^4 in the Taylor series for A_z computed for the monopole doublet (6) for the case $a = 2.5$ cm and $g = 1$ Tesla-(cm)^2. (Lower) The same coefficient computed from 1% random noise. The blue line denotes the rms value as computed using 160 random seeds

trajectory. This is a result of *numerical smoothing*, by which random errors in the values of the magnetic field and scalar potential on the bent box surface are damped as one moves inward toward the reference trajectory.

The same phenomenon also occurs for high-order Taylor coefficients of the vector potential. As an example, one fourth-degree Taylor coefficient for the vector potential of the monopole doublet (6) is shown in the upper plot of Fig. 5. The corresponding Taylor coefficient as computed from 1% relative noise (7) is also shown, which attains a maximum rms value that is 5×10^{-3} relative to the maximum value appearing in the upper figure.

APPLICATION

As an application of this technique, we performed a study of the 35-mm gap design of the Brookhaven NSLS-II dipoles. The dipole is designed to provide 3 GeV electrons with a bend of 6 degrees. Based on the use of Opera 3D, Brookhaven provided data for both the field $\boldsymbol{B}$ and the scalar potential ψ on a grid with

$$x \in [-0.06, 0.06], \quad y \in [-0.016, 0.016], \quad z \in [-1.8, 1.8]$$

and spacing

$$h_x = h_y = h_z = .002.$$

Here all quantities are in meters.

The map computation in BMAP3D was performed using a bent box with height 0.024 m and width 0.1 m. The length of the arc segment was 3.22 m, and the length of each straight leg was 0.1 m. For preliminary fitting, the box was taken to be nearly straight (with a bending angle of 0.6 degrees). As a numerical test, the interior magnetic field was computed in BMAP3D (using $\mathbf{B} = \nabla \times \mathbf{A}$) at several interior grid point locations. This solution for the interior field, which is obtained using only field and potential data on the surface of the bent box, was then compared to the original data at each grid point. Figure 6 displays the computed value of the vertical field B_y off-axis at $(x, y) = (0, 0.2)$ cm along the length of the dipole. Note that the fitted field correctly captures the fringe-field behavior, and the maximum error obtained along the line shown was $|\mathbf{B}_{data} - \mathbf{B}_{fit}|/|\mathbf{B}|_{peak} = 4 \times 10^{-4}$.

As a second test, Fig. 7 shows the reference trajectory through the dipole as computed using BMAP3D, together with a reference trajectory that is computed using numerical integration based on magnetic field data interpolated from the grid. Using the numerically determined Taylor coeffi-

ISBN 978-3-95450-136-6

Copyright © 2015 CC-BY-3.0 and by the respective authors

cients of A_x, A_y, and A_z, a transfer map was computed about this reference trajectory through third order.

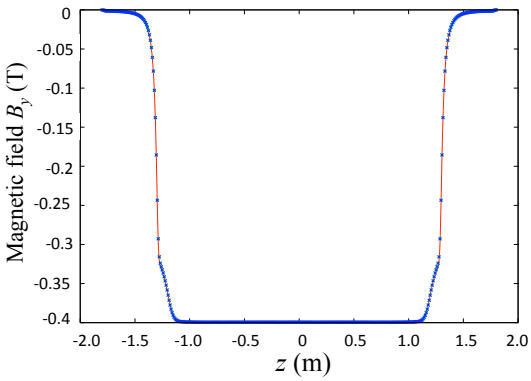

Figure 6: Fit obtained to proposed NSLS-II dipole vertical field using the bent box of Fig. 1. The solid line is a linear interpolation through numerical data provided by OPERA-3d. Dots indicate values computed from surface data using BMAP3D.

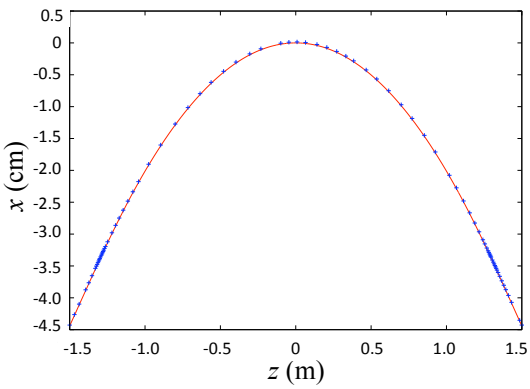

Figure 7: Reference trajectory through the NSLS-II dipole vertical field. (Solid) Reference trajectory computed by BMAP3D using data on the surface of a bent box. (Dots) Reference trajectory computed by numerical integration through magnetic field data on a mesh.

CONCLUSIONS

A parallel code BMAP3D has been developed for computing third-order symplectic transfer maps based on 3-dimensional magnetic field data on a grid, as provided by various 3-D finite element field codes. The method involves fitting field data onto a boundary surface and continuing inward to obtain **A** and its Taylor coefficients in a neighborhood of the beam design trajectory. If desired, the code can produce both **A** and **B** at any interior point, together with Taylor coefficients about this point through 4th and 3rd order, respectively. These quantities can be exported for use with other charged-particle optics codes. The surface-fitting procedure has several distinct advantages:

- The method is based on a smooth (analytic) representation of the interior magnetic field that exactly satisfies Maxwell's equations. One may verify that $\nabla \cdot \mathbf{B} = 0$ and $\nabla \times \mathbf{B} = 0$ at each interior point to within machine precision.
- The error is globally controlled. Each component B_x, B_y, and B_z of both the exact and computed fields satisfies the Laplace equation. Therefore their difference, the error field, also satisfies the Laplace equation, and must take its extrema on the boundary. The fitting error on the boundary is controlled, and the interior error must therefore be even smaller.
- Interior values inferred from surface data are relatively insensitive to errors/noise in the surface data. In general, the sensitivity to noise in the data decreases rapidly (as some high inverse power of distance) with increasing distance from the surface, and this property improves the accuracy of the high-order interior derivatives needed to compute high-order transfer maps.
- Unlike a truncated Taylor map, the computed transfer map in factorized Lie form is exactly symplectic [9].

Using tools such as BMAP3D and those described in [1]-[4], one may obtain a realistic high-order transfer map for an entire accelerator or storage ring without the uncertainties associated with the use of only approximate field models.

ACKNOWLEDGMENTS

This work is partially supported by the U.S. Department of Energy and made use of computer resources at the National Energy Research Scientific Computing Center.

REFERENCES

[1] M. Venturini and A. Dragt, Nucl. Instrum. and Meth. A 427, 387 (1999).

[2] S. Manikonda and M. Berz, IJPAM **23**, 365 (2005).

[3] D. Abell, Phys. Rev. ST Accel. Beams 9, 052001 (2006).

[4] C. Mitchell and A. Dragt, Phys. Rev. ST Accel. Beams 13, 064001 (2010).

[5] C. Mitchell, "Calculation of Realistic Charged-Particle Transfer Maps," Ph. D. thesis, University of Maryland, College Park (2007), `http://www.physics.umd.edu/dsat/`.

[6] J. Stratton and L. Chu, Phys. Rev. **56**, pp. 99-107 (1939); J. Stratton, *Electromagnetic Theory*, McGraw-Hill Book Co., Inc. New York (1941).

[7] C. Mitchell and A. Dragt, in Proceedings of PAC2011, New York, NY, March 2011 (2011).

[8] A. Dragt, T. Stasvevich, and P. Walstrom, in Proceedings of PAC2001, Chicago, IL, June 2001, p. 1776 (2001).

[9] A. Dragt, *Lie Methods for Nonlinear Dynamics with Applications to Accelerator Physics*, University of Maryland Technical Report (2009), `http://www.physics.umd.edu/dsat/`.

Copyright © 2015 CC-BY-3.0 and by the respective authors

ISBN 978-3-95450-136-6